

# 1 Balloon drift estimation and improved position estimates for 2 radiosondes

3 Ulrich Voggenberger<sup>1</sup>, Leopold Haimberger<sup>1</sup>, Federico Ambrogi<sup>1</sup>, Paul Poli<sup>2</sup>

4 <sup>1</sup>Department of Meteorology and Geophysics, University of Vienna, Vienna, 1090, Austria

5 <sup>2</sup>European Centre for Medium-Range Weather Forecasts, Bonn, Germany

6 *Correspondence to:* Ulrich Voggenberger (ulrich.voggenberger@univie.ac.at)

## 7 **Abstract.**

8 When comparing model output with historical radiosonde observations, it is usually assumed that the radiosonde has risen  
9 exactly above its starting point and has not been displaced by the wind. This has changed only relatively recently with the  
10 availability of Global Navigation Satellite System (GNSS) receivers aboard the radiosondes in the late-1990s, but even then  
11 the balloon trajectory data were often not transmitted, although this information was the basis for estimating the wind in the  
12 first place. Depending on the conditions and time of year, radiosondes can sometimes drift a few hundred kilometres,  
13 particularly in the mid-latitudes during the winter months. The position errors can lead to non-negligible representation errors  
14 when the corresponding observations are assimilated.

15 This paper presents a methodology to compute changes in the balloon position during its vertical ascent, using only limited  
16 information, such as the vertical profile of wind contained in the historical observation reports. The sensitivity of the method  
17 to various parameters is investigated, such as the vertical resolution of the input data, the assumption about vertical ascent  
18 speed of the balloon, and the departure of the surface of the Earth from a sphere. The paper considers modern GNSS sonde  
19 data reports for validation, for which the full trajectory of the balloon is available, alongside the **reported** **estimated** wind.  
20 Evaluation is also conducted by comparison with ERA5 and by conducting low-resolution data assimilation experiments.  
21 Overall, the results indicate that the trajectory of the radiosonde can be accurately reconstructed from original data of varying  
22 vertical resolution and that the more accurate balloon position reduces representation errors, and, in some cases, also systematic  
23 errors.

## 1 Introduction

Prior to the availability of remote sensing techniques, upper-air measurements of air motions were widely collected using Lagrangian perspectives, with weather balloons (e.g., Dutton, 1986). The uncertainty of such upper air observations depends not only on the measurements themselves but also on the availability and quality of associated metadata and measurement position: this is generally associated with so-called ~~representation~~~~representativeness~~ errors (e.g., Kitchen, 1989). As weather balloons drift with the wind during their travel, including ascent, they can thus be displaced over large distances; ~~(like Figure 1), shows:~~ in some cases more than 400 km from their launch base (e.g., Seidel et al., 2011). Precise knowledge of the balloon position is particularly important in regions of steep horizontal gradients, e.g. near mountain ranges or near jet streams. Tschannett (2003) and Steinacker et al. (2005) noted that apparent superadiabatic vertical lapse rates in Foehn events disappeared after the balloon displacement had been taken into account. For operational monitoring, detailed information regarding the balloon trajectory was generally not recorded or not transferred via the data distribution networks until the advent of Global Navigation Satellite Systems (GNSS). Even later, when GNSS sensors became available, the information collected was often not transmitted, although the wind data was calculated directly from it (WMO, 2021), ~~as there was no available space for it. The drift information could not be transmitted in the alphanumeric codes. This became possible with the (ongoing) migration from alphanumeric codes to Binary Universal Form for the Representation of meteorological data (BUFR), allowing also the reporting of many more levels in the vertical (Ingleby et al., 2016).~~ Only since the mid-2010s is the balloon drift taken into account in modern observation processing of GNSS sondes, with beneficial results (Ingleby, 2018).

Radiosonde measurements are used in a variety of applications, including near-real-time by forecasters and Numerical Weather Prediction (NWP), but also for air pollution or other scientific investigations, including climate monitoring (e.g., Dabberdt and Turtiainen, 2015). The production of climate reanalyses that directly assimilate radiosonde observations, such as ERA5 (Hersbach et al. 2020), is expected to benefit from more accurate historical balloon position data, similarly to NWP. In this regard, the location precision of the assimilated measurements should be commensurate with the horizontal resolution (~10 to 20 km globally) of future reanalyses. At such resolutions, assuming vertical ascents for a balloon that is displaced by a couple of hundred kms would amount to comparing the balloon measurements with model values that are 10 or more grid boxes away, which is clearly suboptimal. Resolving this situation requires, for historical soundings, to reconstruct the balloon trajectories from the little information that is available (Stohl, 1998). In many cases, this information only consists in the vertical profile of wind, as discussed later in the paper.

~~The present paper presents a method to calculate the balloon drift from historical radiosonde ascent data.~~ Section 2 describes the data and ~~a method to calculate the balloon drift from historical radiosonde ascent data~~~~methodology~~. Details of the technical implementation, with python code and test data, are provided in section 3. Section 4 presents ~~validation~~~~verification~~ results, including ~~from~~ several sensitivity analyses to explore the robustness and accuracy of the approach. Sections 5 and 6 show

58 evaluation results, using two different approaches, whereby the beneficial impact of the more accurate balloon position is  
59 demonstrated. Section 7 includes a discussion and conclusions.

## 60 **2 Data and methodology**

### 62 **2.1 Radiosonde data**

63 Radiosonde data used in this work are obtained from the Integrated Global Radiosonde Archive (IGRA), Version 2 (Durre et  
64 al., 2016) and via the Copernicus Climate Change Service (C3S) Climate Data Store (CDS). High-resolution radiosonde data  
65 used for ~~validation~~~~verification~~ are obtained in BUFR (~~Binary Universal Form for the Representation of meteorological data~~)  
66 format from the ~~National Centers for Environmental Information~~~~University of Wyoming Atmospheric Science~~ Radiosonde  
67 Archive (~~NOAA NCEI~~~~UWYO~~).

68  
69 The quality of the available wind data depends on their encoding and the method used to track the balloons. Measuring  
70 techniques for upper air winds have changed significantly over time, with a clear general trend towards improvements in  
71 quality, thanks to removal of procedural errors, in particular (e.g., Crutcher, 1979), noting also improvements in the accuracy  
72 of encoding, with evolution of the data formats. All these changes are described in the WMO Publication Nr. 8, Guide to  
73 Meteorological Instruments and Methods of Observation, published since 1954 by the WMO Commission for Instruments and  
74 Methods of Observation (CIMO; WMO, 2021). Regarding changes in the measurements of wind and balloon positions, there  
75 are three important distinctions to be made.

76  
77 The first distinction concerns the sensing apparatus: non-GNSS versus GNSS sondes. ~~Early observations used only ground-~~  
78 ~~based tracking, e.g., by theodolite, which was fairly accurate but could lose the balloon early during cloudy or strong wind~~  
79 ~~conditions, and relied on an assumed ascent rate if, like in most cases, a single theodolite was used (e.g., Favà et al., 2021).~~  
80 ~~From the mid-1950s onward, radar tracking or radio-positioning of the radiosonde became standard. Wind was then calculated~~  
81 ~~from the measured position and time differences.~~

82 ~~In the 1990s, GNSS modules were introduced, which~~~~The latter sondes~~ can track the horizontal and vertical position of ~~the~~  
83 ~~balloon and~~ the sensor at high frequency, thanks to improvements and miniaturisation of the electronics. The resulting data  
84 ~~were~~~~are~~ then used to calculate the wind variable in the data set. ~~Early observations used only ground-based tracking, e.g., by~~  
85 ~~theodolite, which was fairly accurate but could lose the balloon early during cloudy or strong wind conditions, and relied on~~  
86 ~~an assumed ascent rate if, like in most cases, a single theodolite was used (e.g., Favà et al., 2021). From the mid-1950s onward,~~  
87 ~~radar tracking or radio-positioning of the radiosonde became standard. In the 1990s, GNSS modules were introduced, but~~  
88 the position data were not transmitted to the global network and are therefore not available in the used input data-bases in most

89 cases until 2014.

90 The higher frequency of observations exchanged in recent years can expose the pendulum motion of the sonde beneath the  
91 balloon in its observed position (Ingleby et al, 2022). In our experimental cases, we did not observe any effect of the pendulum  
92 motion, its magnitude is much smaller than the displacements, suggesting it does not appear to need to be taken into account  
93 to first order.

94  
95 The second aspect is the determination of altitude. Prior to GNSS observations, altitude was determined by three different  
96 methods: ascent speed estimation, pressure sensors and vertical radar or radio-positioning, with continued efforts to increase  
97 the quality of observations over time. Ascent speed can be affected by many factors, and Murillo et al. (2005) estimated a  
98 scatter in linear ascent rates of about 5% about the mean value for pilot balloons, after using double theodolites to conduct  
99 measurements to measure the balloon height during ascent.

100  
101 The third aspect is the data format used for transmission. Essentially two main message systems have been used to transmit  
102 the observed radiosonde data: Traditional Alphanumeric Code (TAC) and BUFR. The main difference is that ~~BUFR~~~~the latter~~  
103 ~~allows for not only has~~ a much higher vertical resolution (up to 1 second frequency, corresponding to approximately 5 m  
104 altitude ~~difference for ascents used in comparison~~), but also a higher coding precision. The BUFR messages report wind  
105 direction with a resolution of 1 degree, whereas TAC messages report wind direction to the nearest 5-degrees. Also time and  
106 three-dimensional position information is only transmitted via BUFR but not with TAC. TAC messages typically also include  
107 data only on mandatory and significant levels. Mandatory levels are a set of predefined pressure levels. Significant levels are  
108 added as needed before transmission so that the wind speed does not deviate by more than 5 m/s from linearly-interpolated  
109 values, according to the above-cited WMO CIMO guide.

110 There are also thermodynamically significant levels, which refer to specific levels of atmospheric pressure at which significant  
111 changes in temperature, humidity or other thermodynamic properties occur. Most transmitted radiosonde profiles include some  
112 of these.

## 113 2.2 Quality control

114 The following steps are taken to exclude outliers:

- 115 • The wind speed is limited to 150 m/s, a value that is rarely reached, even in strong upper-level jets.
- 116 • The temperature is limited to values between 173 K and 373 K.

117 Observations that fall outside these limits are not processed further, to avoid degrading the quality of the output (balloon  
118 trajectory).

119 It was investigated whether additional quality control measures would improve performance and the validation of the RMSE  
120 differences discussed in section 5. To improve outlier removal, we filtered the observations based on the 1st and 99th  
121 percentiles of the observations minus the background from the ERA5 feedback. This was completed in two stages: once for

122 ~~each level, and then again for the entire set of available wind speed and temperature data. However, neither of the two versions~~  
123 ~~improved the RMSE differences. Rather, we found that the background departures were often large enough to be discarded~~  
124 ~~just in the interesting cases of strong but plausible displacements. Therefore, we concluded that such additional quality controls~~  
125 ~~did not affect our results. However, the results presented in section 6 include the standard additional quality controls applied~~  
126 ~~during data assimilation experiments, as applied in the used. These quality controls are those of the data assimilation system,~~  
127 ~~as detailed in the technical documentation published by ECMWF (2023).~~

129 ~~Filtering input data based on the number of available observations per profile is recommended. A profile should not be too~~  
130 ~~coarse and should not start too high above the ground, as this ensures that the calculated trajectory remains a good~~  
131 ~~representation of reality. For the experiments conducted in this study, the limit for the initial observation was set at 1500 m~~  
132 ~~above the release station height. If the vertical distance between the observation and starting point is larger, the~~  
133 ~~displacement is not calculated.~~

134 ~~The same applies when there is no data between a mandatory pressure level and the third second next mandatory level. In order~~  
135 ~~to show the trajectory accurately, this gap was considered too large.~~

**Kommentiert [1]:** COMMENT: This formulation suggests that case never happened. Is this what you meant?

**Kommentiert [2R1]:** No, I'll reformulate that!

**Kommentiert [3]:** This is mentioned again further down, thus I remove it here.

### 137 2.3 Estimation of the balloon trajectory

138 The balloon position is calculated relative to the launch position (so-called base coordinates), as latitude displacement and  
139 longitude displacement (decimal degrees). For each vertical level, these two values can be added to the base coordinates to  
140 obtain the new (latitude, longitude) position at the given level. The same approach applies to the reconstruction of the  
141 measurement times at all levels. This practice conforms to the BUFR encoding standard.

142  
143 For the position calculation, the same simple physical laws that have been used to derive the reported winds are applied. Only  
144 a few initial parameters are necessary for this:

- 146 • station coordinates or starting point of the sonde, here called base coordinates (latitude and longitude);
- 147 • wind vector (zonal and meridional components, noted respectively  $u$  and  $v$ ), measured by the sonde at different  
148 pressure levels;
- 149 • measurement time ( $t$ ) at different pressure levels.

150  
151 These variables enable calculation of how long the sonde was exposed to horizontal wind, and therefore can be used to estimate  
152 the displacement of the sonde.

153 Especially older datasets often only contain the starting time of the ascent, ~~time information is not available for any of the~~  
154 ~~reported pressure levels but temporal information is not available for all the reported pressure levels.~~

155 To estimate the time elapsed since the release of the balloon, ~~three~~ variables are needed:

- 156
- 157 • the reported pressure levels (generally available from radiosondes) or heights (generally available from so-called
- 158 PILOT balloons, also called PIBAL),
- 159 • the sonde ascent speed.
- 160 • [the surface pressure or station height \(not strictly needed for displacement calculation since first level is typically](#)
- 161 [reported quite close to the surface\)](#)
- 162

163 PILOT or PIBAL profiles provide an estimate of height at each level, from which the time at each level can be reconstructed,

164 assuming a given ascent speed. However, for multivariate soundings (radiosondes reporting temperature and wind), observed

165 pressure is often the only information available regarding the radiosonde vertical position. In such a case, the pressure profile

166 needs to be transformed to a height profile. This can be done assuming a piecewise [constant temperature gradient between the](#)

167 [layers of the profile](#)~~polytropic atmosphere, using the available temperature profile~~. The calculation of the vertical gradient of

168 temperature with respect to altitude from the vertical gradient of temperature with respect to pressure is shown below in

169 **Formulae 1** and **2**. Subsequently, **Formula 3** indicates how this information is used to determine the heights of all pressure

170 levels. If the height information is already available (e.g. PILOT data), those steps can be skipped.

171

172 The vertical resolution of the available data varies. While early ascents often contain even less than the mandatory levels (16

173 levels), recent data in high resolution BUFR are available on 3000 ~~levels or~~ [more levels](#). The sensitivity of displacement

174 calculations to vertical resolution is investigated later in this paper.

175 If a single mandatory level is missing within the ascent range, then the displacements are not calculated; we consider that too

176 much information is missing in such a case. If a level was not mandatory in historical data (e.g. 70 hPa, 250 hPa, 925 hPa),

177 this rule does not apply to the data. However, an early termination of the vertical ascent is not an issue, then the displacements

178 are only calculated up to the highest available level.

179

180 The determination of the sonde's ascent speed is more uncertain. It depends on some variables that are poorly determined or

181 unknown, such as the air vertical wind speed and the weight to buoyancy ratio of the probe and the balloon. Deviations in the

182 filling level of the balloon, the air resistance of the balloon skin, as well as the ambient temperature and the balloon gas

183 temperature further influence the ascent speed. A review of some of these factors was made by Favà et al. (2021).

184

185 Using data from recent sondes, our study of the data with known altitude time series indicates that the rate of ascent varies

186 mostly between 2 and 10 m/s. Within this large range, **Figure 2** shows that the mode of the distribution of ascent speeds is

187 around 5 m/s. **Table 3** further indicates that the interquartile range is 2 m/s (i.e., from 4 m/s to 6 m/s). These findings are

188 consistent with other sources (e.g., Seidel et al., 2011). These statistics represent global fluctuations in the ascent speed of  
189 weather balloons.

190

191 Over short time scales, **Figure 3** indicates the vertical velocity of the probe fluctuates substantially. ~~This is true both within a~~  
192 ~~single ascent and also between different ascents.~~~~This is true for the differences within a single ascent, but also for the~~  
193 ~~differences between different ascents.~~ Near the ground and above the tropopause the fluctuations are largest.

194

195 Given the considerations above for historical balloons, one must recognize that the vertical speed can only be estimated in  
196 most cases, and will always lead to significant deviations as compared to measurements obtained from high resolution ascents.  
197 Note the high vertical resolution shown in **Figure 3** is hardly reached in ascents before the year 2000. This also means that if  
198 only mandatory levels are available, the fluctuations in average ascent speed at each available level are smaller, due to the  
199 longer averaging intervals.

200

201 **Figure 2** and **Figure 3** show that an assumed ascent rate of 5 m/s agrees well with the observed mean value. To counteract the  
202 effects of this fluctuating parameter, an attempt was made to use a height-dependent function instead of a constant speed,  
203 which represents the annual average over more than 100 stations.

204

205 As part of this experiment, a polynomial model was also used to improve the accuracy of the average ascent speed. The  
206 resulting displacements showed, however, very little improvement, indicating that the assumed vertically constant ascent rate  
207 of 5 m/s is a sufficient approximation.

208

209 As a next step it is necessary to calculate the height profile from temperature and pressure information using the [dry-polytropic](#)  
210 [height formula for a dry atmosphere with piecewise constant lapse rate](#) (Alexander, P., 2011). Relative humidity could also be  
211 considered by using the virtual temperature, but, since it is often not available for early ascents and the differences in resulting  
212 displacements are small, the air temperature is used in the equation of state. For the first level, the International Civil Aviation  
213 Organization (ICAO) standard atmosphere lapse rate of -0.0065 K/m is used. For all subsequent steps, the temperature gradient  
214 is calculated directly from the temperature and pressure profile (mean values for each layer “i”).

215

216 The height profile is then used to calculate the time interval spent by the sonde between the noted levels. It can be estimated  
217 using the estimated vertical velocity mentioned earlier.

218 These time intervals are then used to determine the transport of the balloon according to the mean wind inside the layer between  
219 the levels  $i$  to  $i + 1$ , see **Formula 4**.

220

221 Afterwards, this distance is converted into latitude and longitude using either the inverse Haversine method on an assumed  
222 sphere, or the forward transport function on the "WGS84" ellipsoid. The difference between the two transport functions is  
223 found to be practically invisible for smaller observed displacements (see **Figure 4**). Nevertheless, the ellipsoid option is used  
224 as it should deliver higher accuracy results. Finally, the resulting latitudes and longitudes are subtracted from the base  
225 coordinates to obtain the displacements.

226  
227 Particular care is required when using reported wind direction near the North or South Pole. For example, when crossing the  
228 North Pole, a radiosonde in a southerly airflow (prior to the crossing) finds itself in a northerly airflow (afterwards). So far,  
229 only TAC has been used at the South Pole station, which means that the wind components are reported according to the launch  
230 position, not to the actual position, and is thus constant during the ascent. We calculate the displacements in x and y direction  
231 valid at this position and then convert that back to lat/lon positions and displacements. It is important to keep in mind the need  
232 for accuracy when calculating displacements. ~~The displacement calculations IGR-A data have been checked specifically for~~  
233 ~~this issue and no problems/issues were found. The launch site at the South Pole Station, which was used for test purposes,~~  
234 ~~provides accurate wind measurements.~~

235  
236 Although the principle of displacement calculation is similar to the method presented in earlier work on this topic (Laroche  
237 and Sarrazin, 2013), we use different input data for height information. Instead of using the average ascent time for each  
238 standard level, we calculate the times for each available level using the mean lapse rate for the representative layer.  
239 Aberson (2017) applied a similar approach for dropsondes, albeit with a different way of calculating the vertical velocity.  
240 Both of these methods are successful and promising, and for the purpose of this method they have been used as the basis for  
241 reconstructing the trajectories as best as possible.

### 243 3 Implementation and availability

244 The software necessary for the creation of calculated balloon trajectories can be found in the Python package rs-drift:

- 245 • <https://zenodo.org/records/10663306/8421009>
- 246 • ~~<https://pypi.org/project/rs-drift/>~~
- 247 • [https://github.com/UVoggenberger/rs\\_drift/](https://github.com/UVoggenberger/rs_drift/)

248 Examples on how to use it are available in all repositories as an IPython notebook "rs\_drift\_example.ipynb".

249  
250 In addition to the coordinates of the launch site or station in degrees latitude and longitude, the trajectory function requires  
251 profiles of four input variables: temperature [K], pressure [Pa], zonal wind (u) [m/s], meridional wind (v) [m/s]. It accepts only  
252 input which is sorted in ascending order.



```
trajectory = rs_drift.drift.trajectory(lat,lon,temperature,u,v,pressure)
```

The function returns the following output:

```
trajectory == [latitude_displacement, longitude_displacement, seconds_since_start]
```

All those output variables are numpy arrays, with one element for each pressure level - with the same length as the input data.

For PIBAL ascents, the geopotential height must be provided as an additional keyword parameter.

It is possible to experiment with input data. If humidity information is available, the virtual temperature can be used instead of the observed air temperature. Also if more information of the balloon's mean ascent rate is present, this should be used as input in the additional arguments. Any approach including proper quality control of input data that is available should be used to create the best possible estimation of the balloon drift.

The drift of the balloon and sonde compounds is introduced as "displacement" from the starting point (launch site). For simplicity, the displacements can be added to the base coordinates to obtain the vertical profile of positions of the balloon.

#### 4. Validation/Verification with GNSS radiosondes

Validation/Verification per se is only possible when a trusted source can provide a good indisputable reference. Such is the case for modern sondes equipped with GNSS receivers, when it comes to the recovery of the balloon trajectories. For pre-GNSS radiosondes, a similar validation/verification would be possible, if only one had available the information about the balloon trajectory. Unfortunately, this information is available only in rare cases.

The data from the modern GNSS radiosonde data encoded in the recent high-resolution BUFR files are used to verify the systematic and random errors of the calculated displacements at different pressure levels. This data set contains second-by-second records of actual positions of the sonde measured by GNSS in the form of displacements, thus enabling the direct comparison with the calculated displacements.

Figure 4 also shows that the displacements obtained from GNSS and the displacements calculated from the wind data agree quite well. The small deviations likely come from differences between the actual (unknown) and assumed (5 m/s) ascent rate.

Figure 5 provides an overview how large the displacements typically are and gives profiles of uncertainty estimates for the calculated displacements. In the troposphere the RMSE is mostly below 0.02 degrees (2.5 km), in the stratosphere it can be up to 0.1 degrees (12 km). These numbers amount to uncertainties of about one part in five to ten, of the observed variations (RMS), in the example shown. Still, this is much better than just ignoring the displacement.

**Kommentiert [4]:** I think this needs to be mentioned and should be reflected in the software version uploaded to pypy.

285

286 These results were obtained by using as input the high-resolution data. For historical radiosondes, only comparatively low-  
287 resolution information is available (in the form of mandatory plus significant levels).

288 In **Figure 6** and **Figure 7**, the impact of using only mandatory and significant level information is shown. The difference of  
289 displacements in **Figure 6** is minimal, although the displacement is relatively large.

290 **Figure 7** shows a case of larger differences in relative terms. The overall ~~zonal~~ longitudinal displacements are large and the  
291 winds vary strongly with altitude. ~~An issue arises when selecting data points with low representativeness from the ascent,~~  
292 ~~particularly those that are far from the layer average. This can result in less accurate outcomes compared to using averages~~  
293 ~~from less detailed data. Figure 7 provides a good example of this issue with the v component of wind at original resolution and~~  
294 ~~mandatory pressure levels only. Poor representativity of the selected levels—i.e. data points from the high resolution BUFR~~  
295 ~~dataset, far off the mean, may lead to worse results than wind averages between the levels from less high resolution data—see~~  
296 ~~v component of wind original and on mandatory pressure levels only.~~ The method of calculating the displacements itself uses  
297 mean wind speeds within the considered levels. Thus, if the observations are also means of larger vertical height differences,  
298 more or less randomly observed peaks become a smaller source of error.  
299 ~~Figures 6 and 7 respectively show the range of accuracy of the calculated trajectories quite well. The final displacements may~~  
300 ~~differ in quality depending on the quality of the observations, the representativeness of the available levels, and the vertical~~  
301 ~~resolution. Applying the calculated displacements has improved the location of all validation examples. All ascents in the~~  
302 ~~validation examples had displacements, which added value in bringing the observation closer to the true position. The accuracy~~  
303 ~~may vary based on the aforementioned input variables. However, we did not find anythere is no case where not using the~~  
304 ~~displacements would lead to a worsebetter position estimate.~~

305

306 **Figure 8** shows the comparison between the displacements of two different data sets - on high resolution BUFR levels and on  
307 the other hand on mandatory levels only. It can be seen that for this subset of ascents there is still much value in the  
308 displacements for the mandatory levels only version. However, it should be noted that more available levels always lead to  
309 better results and the highest possible number should be used in any case.

310

311 Many of the older observational reports contain temperature and wind data on different levels. Only at mandatory levels both  
312 variables are available. In this case, interpolation can be performed for the points in between. When applied to IGRA data,  
313 wind data are interpolated to [levels of the](#) temperature observations. This allows the input to be maximised to calculate the  
314 best possible displacements.

315

316 **5. Evaluation with ERA5**

317 To evaluate the impact of taking the displacements into account, we compared the observed values from the radiosondes with  
318 the gridded ERA5 data, in one case assuming a strictly vertical ascent, and in the other case assuming an ascent along the  
319 calculated (slanted) trajectory defined by the displacements. The ERA5 fields at hourly resolution ~~and were used at~~  $1^\circ \times 1^\circ$   
320 horizontal resolution, ~~which were then~~ interpolated linearly horizontally to the observations locations defined in either of the  
321 two cases mentioned earlier (vertical or slanted).  
322 These tests and comparisons used the short term forecast of the ERA5 assimilating model, also referred to as "background".  
323 This choice, instead of using ERA5 analyses, was made to try to maintain as much independence as possible with respect to  
324 the observations. This choice should largely avoid possible problems resulting from the fact that the observations are also  
325 assimilated into the ERA5 data, given that many other observations were assimilated alongside radiosondes and also influenced  
326 the analysis state. Experimental comparisons to the ERA5 analyses showed that the analysis data fits significantly better with  
327 the vertical trajectory of observation than with the slanted version. This is to be expected, since radiosondes were assimilated  
328 as vertical profiles in ERA5.

329  
330 **Figure 9** shows the benefit of comparing the radiosonde observations with the *background forecasts* as slanted profiles instead  
331 of vertical profiles. In low layers (below 700 hPa), the displacements are relatively smaller than at higher levels, and therefore  
332 hardly lead to deviations for temperature. In most cases, there is an improvement at levels located above 750 hPa, though at  
333 some stations the improvement is visible already as soon as the sonde reaches 850 hPa, depending on the wind speed and  
334 topography around the station. Typically, the effect is largest in regions with high upper-level wind speeds. Taking the  
335 displacements into account improves the *background* departure statistics between measurements and ERA5 not only for  
336 temperature but also wind and relative humidity (**Figure 10**).

337  
338 For relative humidity, the improvement is confined to levels located below 250 hPa. Above this level, the relative humidity is  
339 generally very low, making it difficult to detect any meaningful difference with respect to the ERA5 background.

340 It is also important to note that some stations, where the RMSE of the ascents do not show signals of improvement in  
341 temperature, often still show improvement in humidity or wind (or vice versa).

342  
343 Considering that *early* radiosonde observations make up a larger part of the total observations for the reanalysis in earlier years,  
344 one might think that especially for these years the displacements are more relevant. The data investigation reveals that  
345 improvements of the departure statistics are not greater for earlier ascents than for more recent ascents. The reason might be  
346 that reanalysis fields before the satellite era are more strongly dependent on radiosondes. At these times few other upper-air  
347 observations were available, and radiosonde data were assimilated assuming vertically straight ascents. However, the density  
348 of the input data and the general quality of the reanalysis increased over the time, while the bias in measurements of the

Formatiert: Schriftart: Kursiv

Formatiert: Schriftart: Kursiv

349 uppermost levels decreased over time. Therefore, the relative importance of representation uncertainties, with respect to the  
350 two other sources of uncertainties in the comparison (radiosonde instrumental uncertainties and ERA5 background  
351 uncertainties), is larger for more recent ascents. **Figure 104** shows that considering the displacements is beneficial, although  
352 to a lesser extent, also in the early days, when little upper air information other than radiosondes was available.

353  
354 Finally, in **Figure 1112** there are the results of a global comparison for the year 2000 - like the previous ones, but calculated  
355 for all the available stations. A positive difference again indicates improvement due to taking the displacements into account.

356  
357 To give a better insight, the differences of the RMSEs are also plotted on a map for the 150 hPa level in **Figure 1213**. Warm  
358 colours show improvement for the respective station by applying the displacements, cold colours show a deterioration.  
359 Improvement clearly predominates for the majority of stations. Deteriorations in quality appear less frequent and of smaller  
360 magnitudes than improvements.

361  
362 **Figure 1314** shows the difference of the ERA5 background eastward wind speed in the 1990s at the station location minus the  
363 same wind speed at the displaced location. The differences are sizable in some regions. For example, the weaker wind speeds  
364 above station locations in China would indicate systematically too high observed wind speeds. This effect is large enough to  
365 explain some of the radiosonde wind minus background wind differences, as pointed out by Tenenbaum et al. (2022). This  
366 stresses again the importance of avoiding position errors in historical radiosonde ascents. Without the adjustments, artificial  
367 trends in wind speed from radiosondes would be introduced in some regions when switching from traditional to GNSS  
368 radiosondes.

## 370 6. Evaluation with data assimilation experiments

371 Desroziers et al. (2005) proposed a method to diagnose uncertainty statistics of observations, in a data assimilation framework.  
372 As indicated in their work, there are important assumptions associated with the approach. Bias contributions aside, the overall  
373 level of uncertainties may be incorrect if, for example, there is significant correlation between observation random uncertainties  
374 and random uncertainties of the background that is used in the data assimilation. A separation of scales is indeed required in  
375 order to disentangle these two uncertainty components. Given the unique importance of radiosondes to inform on the state of  
376 the stratosphere in a background obtained from data assimilation, such as in a reanalysis (e.g., Hersbach et al., 2020), there  
377 may be some components of the uncertainties (such as radiation) that are present, and possibly correlated, in the background  
378 and the observations. For these reasons, we do not use Desroziers' diagnostics in order to assign undisputable uncertainties to  
379 the radiosonde uncertainties. Instead, we use these diagnostics in order to detect any changes in the observation uncertainties,  
380 which include instrument and representativity uncertainties, owing to the effect of balloon drift.

381

382 To this end, we run two data assimilation experiments, using a simplified data assimilation setup. Simplifications are required  
383 in order to make such an undertaking numerically affordable. Otherwise, so-called ‘full’ data assimilation experiments, using  
384 all observations at the maximum resolution, are indeed too costly to conduct, if only for such an evaluation. The simplified  
385 data assimilation setup is based on the ECMWF Integrated Forecasting System (IFS) cycle 48R1 configuration (ECMWF,  
386 2023), using an octahedral reduced Gaussian grid with 159 wavenumbers, or approximately a horizontal resolution of 69 km,  
387 instead of the ECMWF operational configuration which has a resolution of approximately 9 km at present. Also, similarly for  
388 affordability reasons, the experiments only assimilate conventional observations (no satellite observations), the number of  
389 four-dimensional variational (4D-Var) minimizations is reduced from three to two, and the analysis increments are at a  
390 resolution of approximately 210 km (instead of 39 km for ECMWF operations). [The simplified data assimilation setup enables  
391 us to run data assimilation experiments for a duration of two months, 01 June - 31 July 1980.](#)

392

393 The first experiment is the control. It assimilates the radiosonde observations as vertical profiles. The second experiment  
394 assimilates the radiosonde observations ~~as slanted profiles,~~ following the balloon trajectory, when ~~at this information~~ is  
395 available (otherwise the data are assimilated as vertical profiles). [The balloon drift in the assimilation is handled by dividing  
396 the whole ascent into 15-minute sub-profiles \(Ingleby et al., 2018\). In each sub-profile, the latitudes, longitudes, and times are  
397 invariant. In spite of this arrangement, which only partially reflects the true slanted nature of the profiles, we retain the  
398 terminology of “slanted profile” when discussing the results, for clarity within this paper. ~~The simplified data assimilation  
399 setup enables us to run these two experiments for a duration of two months, 01 June – 31 July 1980.~~](#)

400

401 We consider here the radiosonde observations that were assimilated in both experiments, to ensure no difference in results may  
402 be caused by sampling differences. **Table 4** shows the statistics for these data. For the reasons mentioned earlier, the  
403 interpretation of the table focuses on differences between the two experiments, and not on the absolute level of observation  
404 uncertainties determined by Desroziers’ diagnostics. Within 0.1 K, we find no detectable difference between the two  
405 experiments for the ~~pressure-~~levels [located below the 100 hPa pressure level](#). For [levels located higher, i.e. pressures lower](#)  
406 [than 100 hPa](#), one finds that background departures and estimated observation uncertainties are reduced in the experiment that  
407 assimilated the data along slanted profiles. This result is obtained for radiosondes launched from land stations as well as  
408 radiosondes launched from ships.

409

410 The differences may appear as very small and could be discarded as non important, if it was not for the fact that reducing  
411 [observation and representation uncertainties such quantities](#) is generally an impossible task, once observations were collected  
412 and processed already once. The present findings demonstrate that it is possible to generate greater return, in terms of  
413 information content, through a reprocessing of the observations. [The reprocessing enables here to assimilate observations along  
414 a slanted trajectory](#). Furthermore, these are global statistics - see **Figure 1415**. The previous sections indicated that results may

415 vary per launch site. Consequently, the improvements shown here, for global statistics, must hide some greater improvements  
416 at some particular sites - see [Figure 1516](#).

417  
418 [Given previous results indicating a larger effect of the balloon drift during winter seasons \(e.g. McGrath et al., 2006\), and](#)  
419 [given the much greater number of radiosonde stations in the Northern Hemisphere as compared to the Southern hemisphere](#)  
420 [\(e.g., see Figure 12\), the present choice of the data assimilation season \(Northern hemisphere summer, as Choi et al., 2015\)](#)  
421 [represents a conservative approach. An impact of larger magnitude may be expected at different time periods, in particular](#)  
422 [during Northern hemisphere winter.](#)

## 424 7. Discussion and conclusions

425 The verification and evaluation results have shown quite clearly that if at all possible, balloon displacements should be taken  
426 into account for all relevant data assimilation applications to minimise representation errors. Ignoring the possibility to account  
427 for observation location errors on the 100 km scale would be anachronistic, when global or regional reanalysis data sets  
428 approach spatial resolutions finer than 20 km.

429  
430 The method to reconstruct the balloon position presented in this work is limited by a few assumptions and depends on the  
431 vertical resolution of the available profiles, and the conformance of the weather balloons to modern ascent speeds. For the  
432 applications tested, an attempt was made to obtain the best results globally, and a clear positive impact was found, particularly  
433 when comparing to ERA5 in the early 2000s, although positive results were also found at other times (e.g., 1980s). This is also  
434 consistent with other findings in similar settings where trajectory data are used to reduce representation errors (e.g., Laroche  
435 [and Sarrazin, 2013](#)).

436  
437 The data assimilation experimental setup employed here is a simplified one, as compared to what may be used in a present-  
438 day reanalysis configuration such as ERA5. Yet, we observe a positive impact of the balloon drift in terms of reducing the  
439 background departures and the observation uncertainty, using Desroziers' diagnostics, for temperatures in the stratosphere.

440 We expect that [the quality of the corrections made to account for balloon drift when computing background departures impact](#)  
441 [to of using radiosondes at a displaced horizontal position, as compared to using them at a vertical position, would increase](#)  
442 [when the background resolution and/or the background quality is increased. However In addition, assessing the impact of the](#)  
443 [balloon drift sensitivity to the assimilation of other observations Furthermore, we also expect that any positive impact of sonde](#)  
444 [displacement be amplified when satellite observations are used alongside radiosondes would be worth analysing. Increased](#)  
445 [reliance on satellite observations reduces the influence of the radiosonde data and thus the influence of errors in the](#)  
446 [representation of the radiosonde data in the reanalysis. This leads to a comparison with data that is less dependent on the](#)

447 original observation. If this gives a more consistent and evenly distributed improvement, then it should be safe to say that the  
448 comparison with a more satellite-heavy reanalysis is the reason why later comparisons show more improvement.

449 Also, the background for the comparison with earlier data is of lower quality. Therefore, removing the representation error  
450 may show less improvement. However, owing to time and computational constraints, it was not possible to investigate further

451 these effects with full data assimilation experiments at higher horizontal resolution and using all available information, but we  
452 note this would be a useful pursuit.

453  
454 The results of the tests have shown that the method is successful in reconstructing displacements and improving the accuracy  
455 of the atmospheric data. Whilst the additional information provided by the method may not always be a visible improvement  
456 for individual comparisons, it is of significant value when the displacement changes the gridbox of the model being compared.  
457 This has been demonstrated by improved means in the plots and better agreement between observations and ERA5.

458  
459 The value of improving radiosonde observations by reprocessing of the positions was evaluated by conducting reduced-  
460 resolution data assimilation experiments, covering a two-month period in summer 1980. In the future, it would be desirable  
461 that the impact of similar activities that seek to improve the observational record be more regularly evaluated in the generation  
462 of downstream climate products. Such an evaluation should consider a longer time period and include the impact on low-  
463 frequency variability in the products. For products such as reanalyses, obtained via data assimilation, this should entail full-  
464 resolution Observing System Experiments (OSEs). For other types of climate products, including those powered by new  
465 opportunities such as Artificial Intelligence or Machine Learning (e.g., Singh et al., 2022), it is important that mechanisms be  
466 found to evaluate the impact of using the observations and how changes made in their handling affects the outcome.

467  
468 Further experimentation using observation data from the period 2000 - 2020 is crucial and is likely to produce more compelling  
469 outcomes. The effective use of this method for informing future climate reanalysis is one of the main objectives.

470 As the world faces increasing challenges related to climate change, the importance of accurate atmospheric data and the  
471 potential of new methods to improve it cannot be overstated. The use of improved position metadata with radiosonde  
472 observations can account for previously unexplainable phenomena, demonstrating the potential of this method to shed new  
473 light on atmospheric data analysis. In addition, the method has the potential to improve the accuracy of reanalyses and climate  
474 predictions, which are crucial for many socio-economic sectors and the protection of future life.

475  
476 To achieve the optimal representation of the data, precise details regarding time and location must be available for every  
477 observation. One significant issue concerns the TAC format's transmission and storage of data, which often only includes a  
478 nominal timestamp such as 00:00 UTC or 12:00 UTC. However, the actual launch of the respective balloon in most cases took  
479 place 30-60 minutes earlier. The precise time difference from the nominal time is frequently unknown, therefore displacement  
480 information cannot be utilised to its fullest extent. Since temperature can vary by more than 1 K/hour in the boundary layer

Kommentiert [5]: Newly added

481 just due to the diurnal cycle this issue should be addressed. There are well known examples where changes in the sampling of  
482 the diurnal cycle introduced spurious trends into climate data products (Mears and Wentz, 2005). Whenever possible, the  
483 precise launch time should be used. In cases where this information is not available for individual ascents, the time difference  
484 between the nominal and actual launch can [often](#) be determined from earlier or later ascents. Operators are normally advised  
485 to minimise the variation throughout the launch procedure and, therefore, launch balloon sondes at the same time every day.  
486

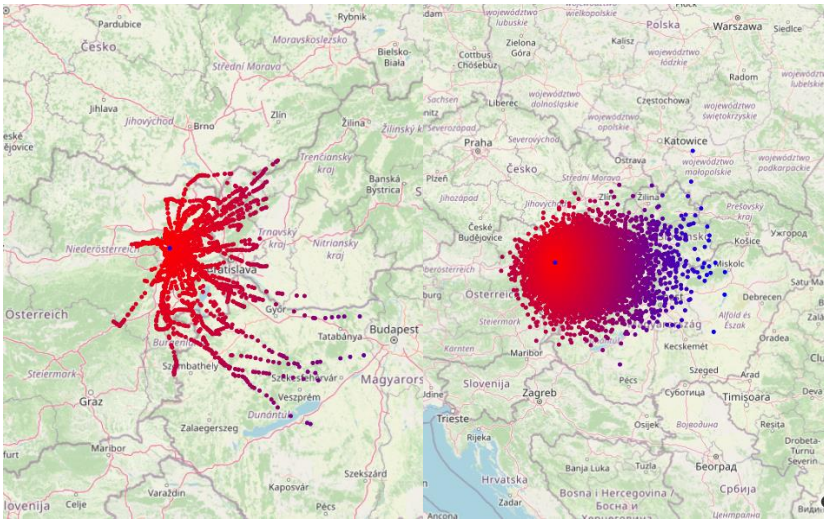
487 Additional work to better understand the causes of variation in balloon ascent speeds (e.g., Zhang et al., 2019) could help  
488 further improve the results. Also, given all the uncertainty sources, it could be possible to generate an ensemble of trajectories  
489 for each ascent.

490 The same approach can be used to reprocess rocket or drop-sondes, ozone-sondes or any other in-situ sonde carried by the  
491 wind, provided the necessary information is available. Taking into account the accurate balloon position would also be  
492 beneficial when comparing radiosonde observations with GNSS radio occultation (RO) observations (Gilpin et al. 2018).  
493 While the slanted profile of the RO data is considered, radiosonde data is frequently presumed to move vertically only.  
494

495 In conclusion, the development and testing of the method for [reconstructing displacements based on the wind](#)  
496 ~~[profile](#)~~[reconstructing displacements based on the reversed calculation of wind speed and direction](#) shows promising results.  
497 The results presented in this paper suggest taking balloon displacements into account when producing meteorological or  
498 climatological data based on upper-air in situ balloon-borne observations.  
499

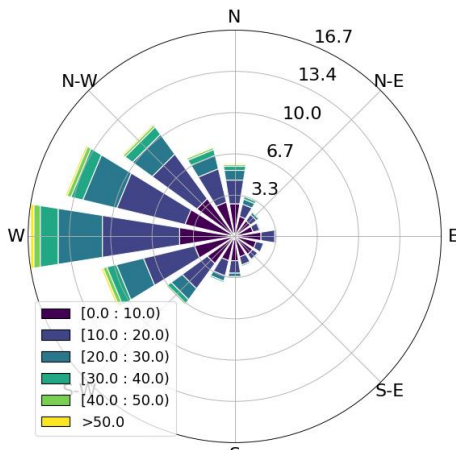


500 Appendices



501  
502

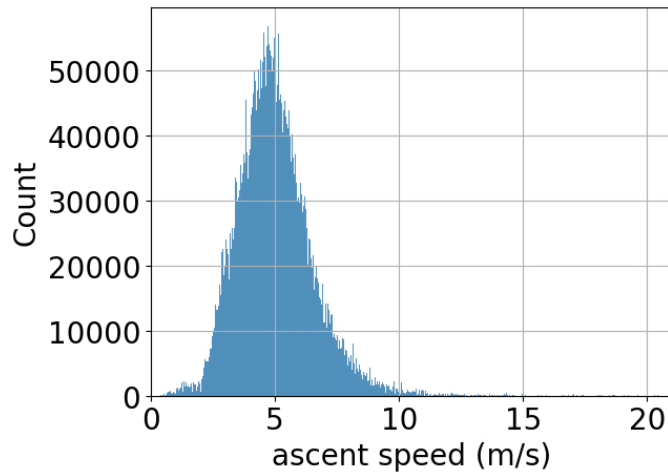
© OpenStreetMap contributors 2023. Distributed under the Open Data Commons Open Database License (ODbL) v1.0.



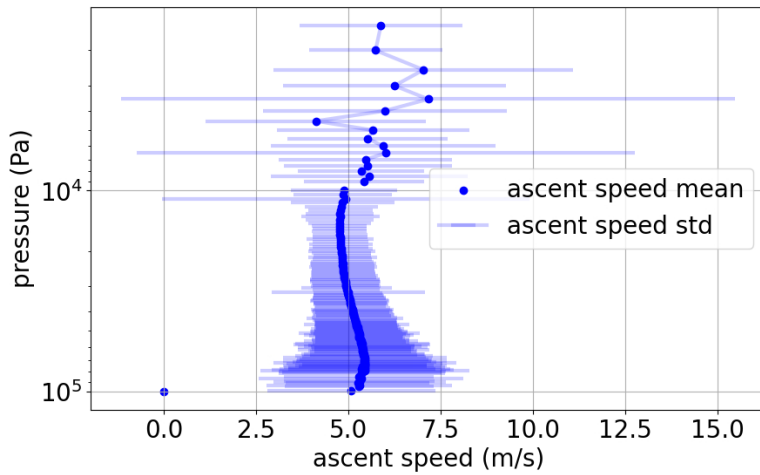
503  
504  
505

Figure 1: Balloon displacements for station Vienna Hohe Warte, Austria (WIGOS ID 0-20001-0-11035, central blue dot) red to blue with increasing distance. Note the area covered is non-isotropic around the launch site. Left panel: Trajectories of all radiosonde

506 ascents during the year 2000. Right panel – maximum displacements of all available ascents for all years between 1950 and 2021.  
507 Lower panel: windrose of Vienna Hohe Warte station for all available wind data. Colour indicates wind speed [m/s], radius indicates  
508 frequency distribution [%] of direction, from where the wind comes from ~~wind-direction~~ (sectors) and wind speed (colors).  
509

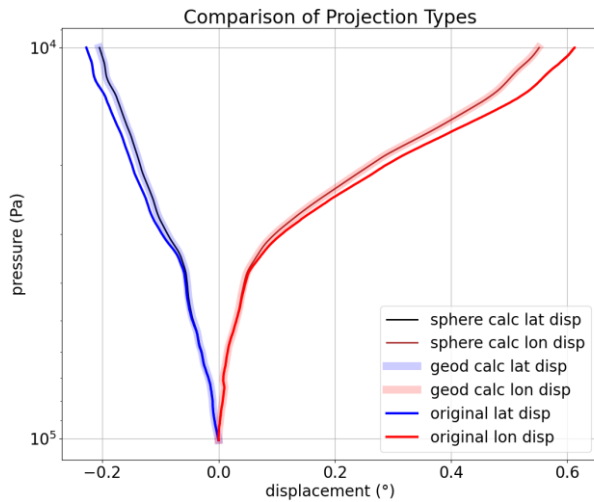


510  
511 **Figure 2: The observed ascent speeds from a sample of approximately 10 million BUFR encoded observations with known altitude**  
512 **time series in 2020.**



513  
514  
515

Figure 3: Mean ascent speed with standard deviation bars for all radiosonde ascents from Riverton USA, in 2020, derived from high resolution BUFR data.



516  
517  
518  
519

Figure 4: Calculated displacements (black and brown for spherical earth, thick light blue and red for WGS84). Observed displacements stored in BUFR displacements (blue and red) are included for comparison. Tallahassee, Florida - USA 2020.05.31 23:19:00

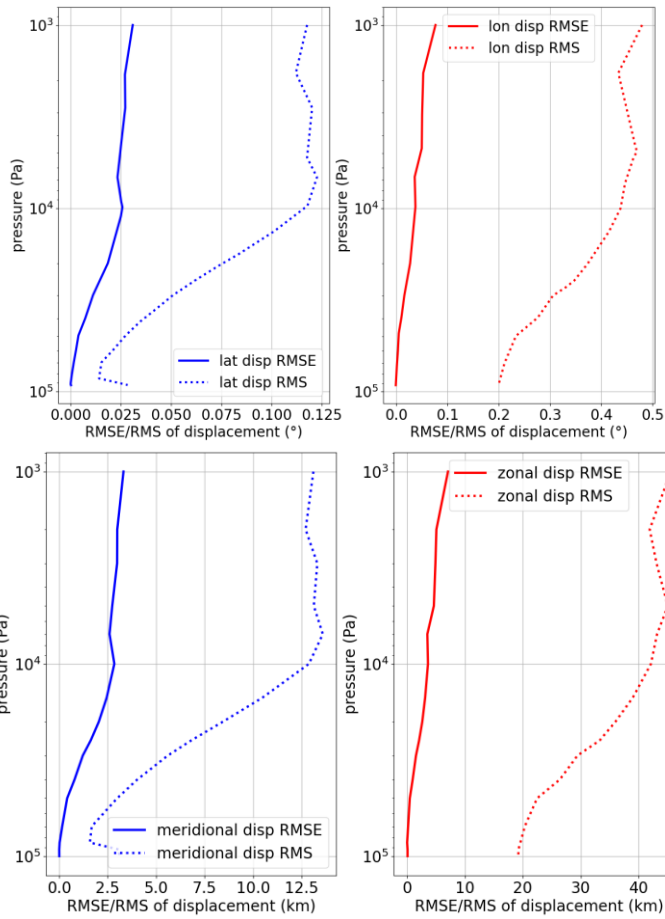
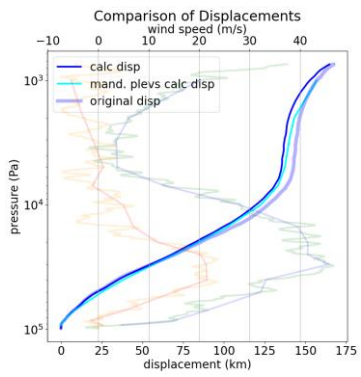
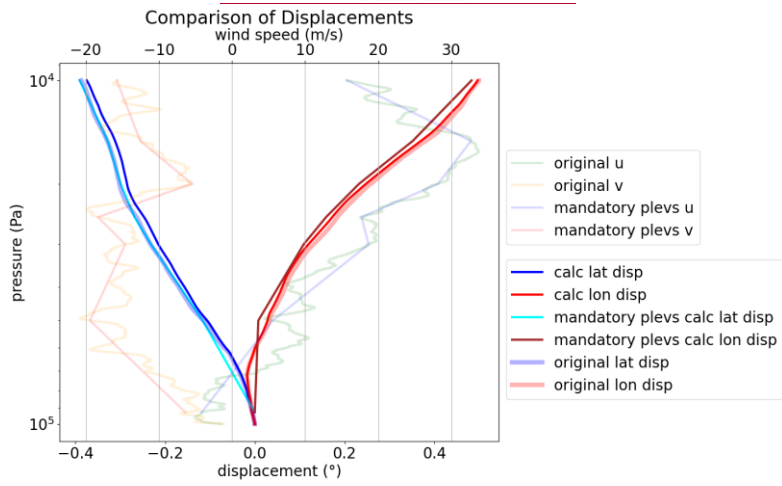


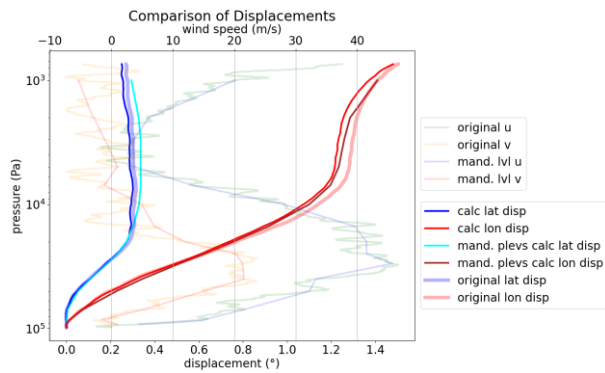
Figure 5: RMS of **meridional** latitude (blue dotted) and **zonal** longitude (red dotted) displacements and RMSE between observed (from GPS) and modelled displacements (solid blue and solid red, respectively). The samples contain all BUFR encoded ascents in the summer months of 2020 (more than 10000).

525



526

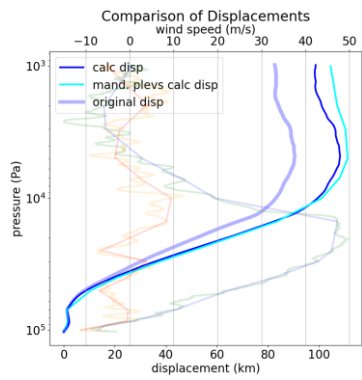




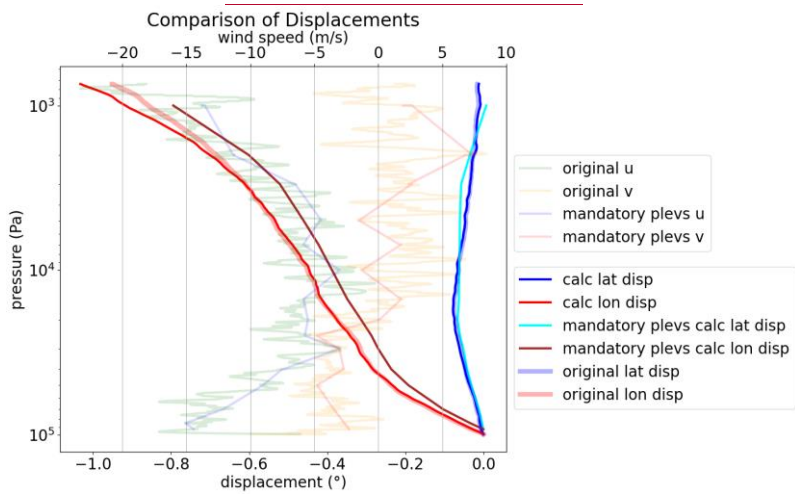
527  
 528 **Figure 6: Vertical profiles of displacements (starting at zero at surface), calculated from observed winds (thin lines) or taken from**  
 529 **BUFR thick light lines. The profiles of observed wind (thin light colors) are plotted to the upper x axis - Peachtree City, Georgia -**  
 530 **USA 31.01.2021 23:24:00. Left panel: overall displacements in km, right panel: lat and lon displacements in degrees as encoded in**  
 531 **BUFR. Figure 6: Vertical profiles of displacements (starting at zero at surface), calculated from observed winds (thin lines) or taken**  
 532 **from BUFR thick light lines. The profiles of observed wind (thin light colors) are plotted to the upper x axis - Green Hill, Tennessee**  
 533 **-USA 31.05.2020 23:00:00**  
 534

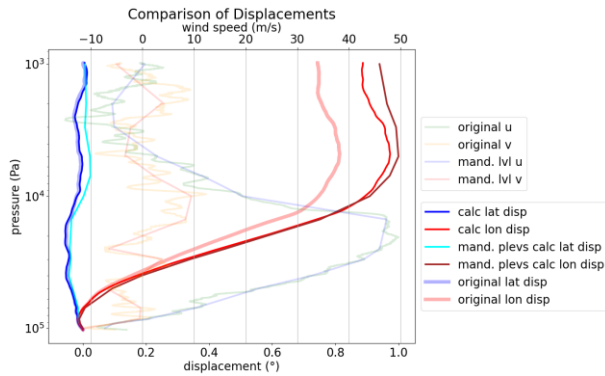
Formatiert: Schriftart: 9 Pt.

535



536





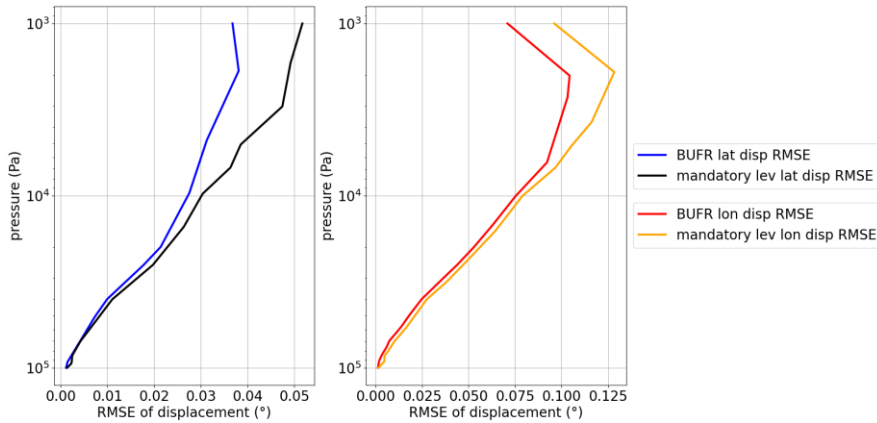
537  
538  
539  
540

Figure 7: Vertical profiles of displacements (starting at zero at surface), calculated from observed winds (thin lines) or taken from BUFR thick light lines. The profiles of observed wind (thin light colors) are plotted to the upper x axis - Ishigaki, Okinawa - Japan 2019.12.31 23:31:00 . Left panel: overall displacements in km, right panel: lat and lon displacements in degrees as encoded in BUFR.

541  
542  
543

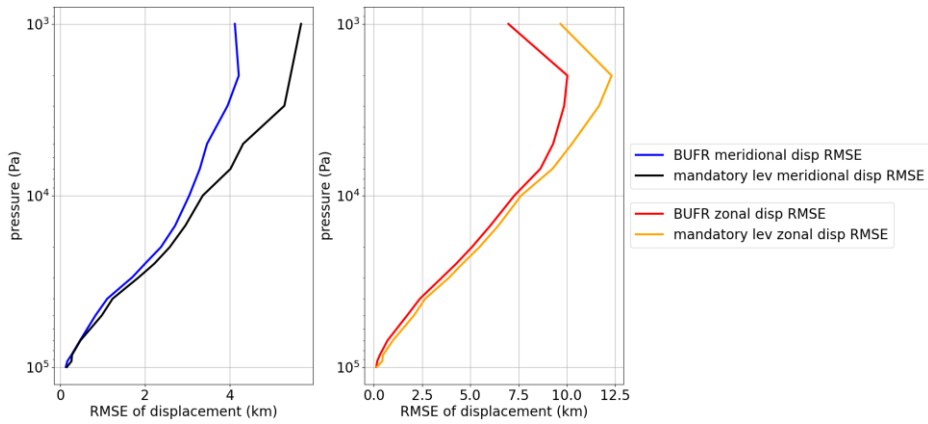
Figure 7: Vertical profiles of displacements (starting at zero at surface), calculated from observed winds (thin lines) or taken from BUFR thick light lines. The profiles of observed wind (thin light colors) are plotted to the upper x axis - St. Paul Island Airport, Alaska - USA 2020.05.31 23:01:00

544

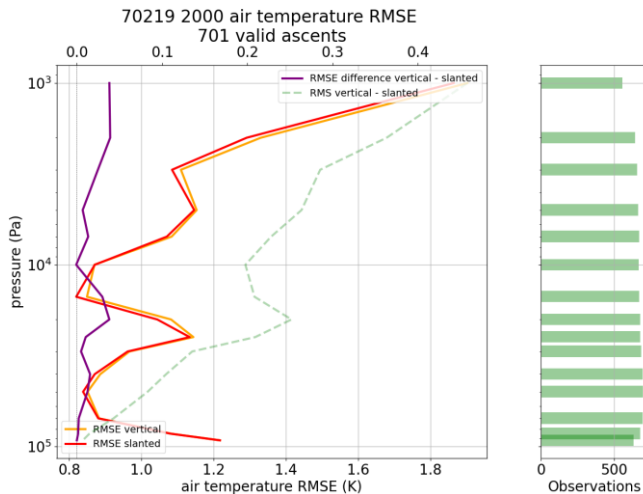


545





546  
 547 **Figure 8:** RMSE between observed and modelled displacements of **meridional latitude** (left panel) and **zonal longitude** (right panel)  
 548 **components**, averaged over all stations available in October 2014, one of the first months with a sizable number of high-resolution  
 549 BUFR encoded profiles. Blue and red are RMSE profiles obtained by using the full vertical resolution of BUFR observations, black  
 550 and orange are RMSE profiles, and obtained by using only mandatory level information.  
 551



552  
 553 **Figure 9:** Bethel Airport, Alaska all 2020 ascents. RMSE (obs - ERA5) of base coordinate temperatures minus sonde temperatures  
 554 (orange) and RMSE (obs - ERA5) of displaced temperatures minus sonde temperatures (red), also RMS of displaced minus base  
 555 (green dashed) to show the magnitude of difference between base and displaced temperatures. Positive difference between orange  
 556 and red graphs (purple line, upper x axis) shows improvement due to more accurate balloon position. Green bars on the right  
 557 indicate sample sizes at different levels.

558

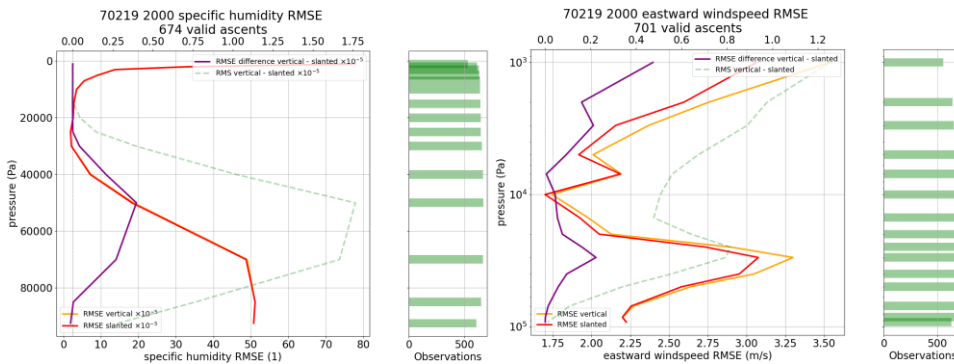


Figure 10: Bethel Airport, Alaska all 2020 ascents. Left: RMSE (obs - ERA5) of vertical specific humidity minus sonde specific humidity (orange) and RMSE (obs - ERA5) of slanted specific humidity minus sonde specific humidity (red). Right: RMSE (obs - ERA5) of vertical eastward wind minus sonde eastward wind (orange) and RMSE (obs - ERA5) of slanted eastward wind minus sonde eastward wind (red). Positive difference between orange and red graphs (purple line, upper x axis) shows improvement due to more accurate balloon position.

559

560

561

562

563

564

565

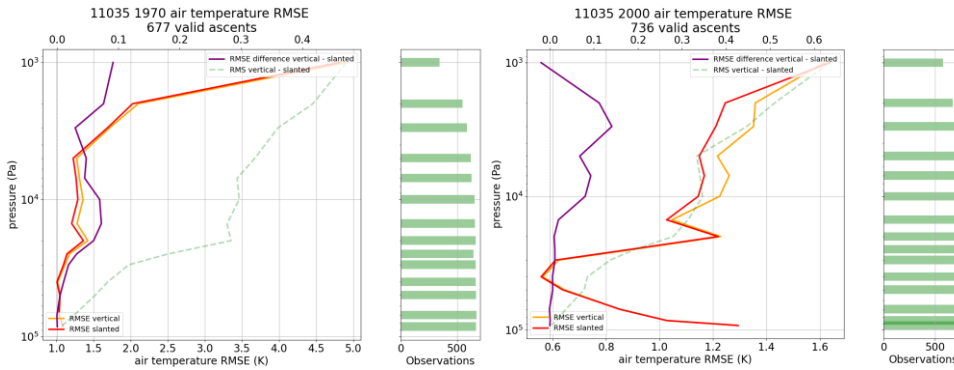


Figure 104: Vienna Hohe Warte, Austria - Left: 1970 all ascents, Right: 2020 all ascents. Different x-axes scales are used. RMSE (obs - ERA5) of vertical temperature minus sonde temperature (orange, lower x-axis) and RMSE (obs - ERA5) of slanted temperature minus sonde temperature (red, lower x-axis). Positive difference between orange and red graphs (purple line, upper x axis) shows improvement due to more accurate balloon position.

566

567

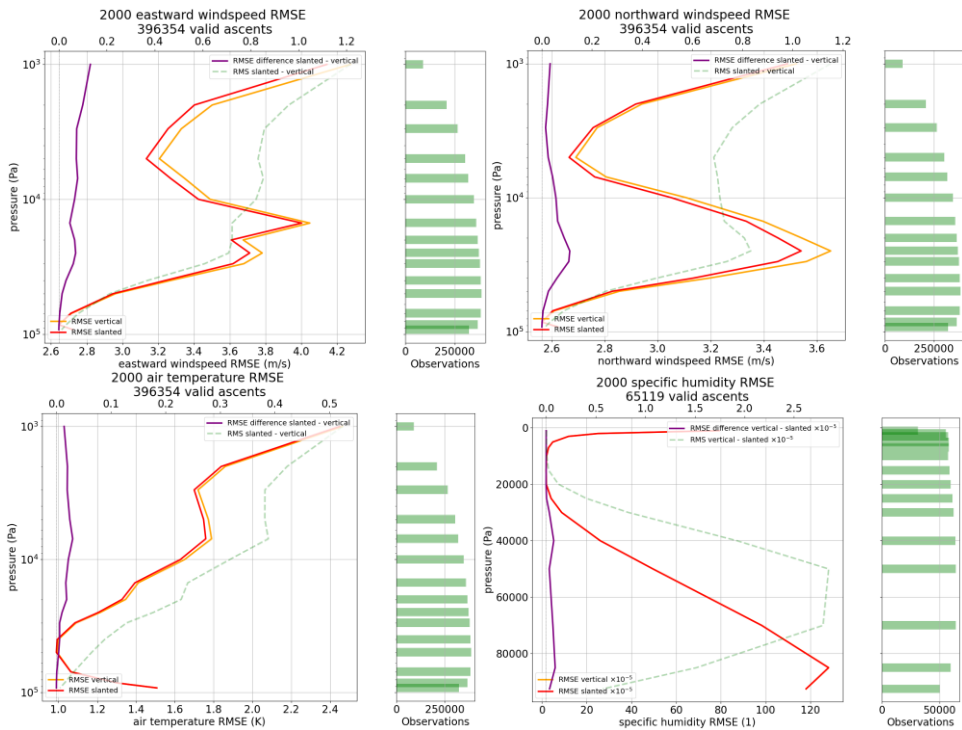
568

569

570

Formatiert: Abstand Nach: 10 Pt., Rahmen: Oben: (Kein Rahmen), Unten: (Kein Rahmen), Links: (Kein Rahmen), Rechts: (Kein Rahmen), Zwischen : (Kein Rahmen)

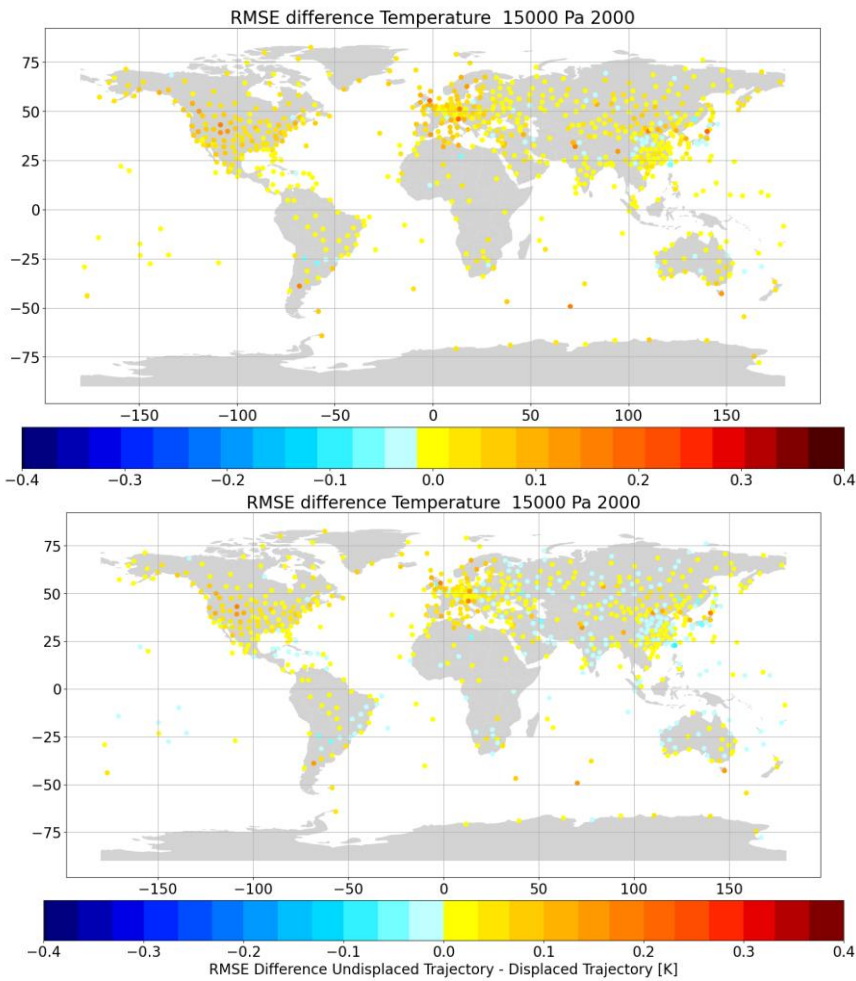
571  
572



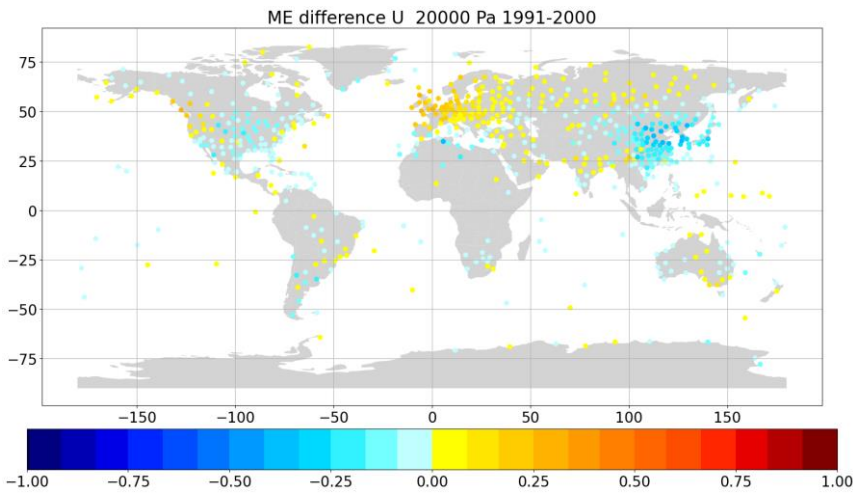
573

574  
575  
576  
577  
578  
579  
580  
581  
582

Figure 1142: Global RMSE (obs - ERA5 background) assuming vertical ascents (orange) and RMSE (obs - ERA5 background) from reconstructed slanted ascents (red), calculated from all available ascents of year 2000. The differences between orange and red graphs (purple line, upper x axis) shows how much the better balloon position improved the temperature data (positive = improvement). The “RMS vertical - slanted” (green dashed line, upper x axis) indicates how much the ERA5 background varies on average between the vertical and slanted balloon profiles. - Top left: u wind component; Top right: v wind component; Bottom left: temperature; Bottom right: specific humidity in kg/kg (note scaling factor  $10^{-5}$ ).

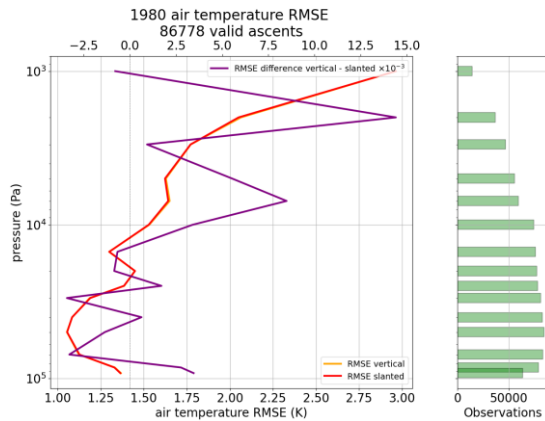


583  
584  
585 **Figure 13: Global stations difference of temperature [K] observation RMSE (obs - ERA5) when compared to background at station**  
586 **coordinates minus the temperature observation RMSE (obs - ERA5) when compared to background at displaced position - Positive**  
587 **values indicate improvement due to more accurate balloon position. All available observations at 150 hPa averaged over all ascents**  
588 **in the year 2000.**



589  
590  
591

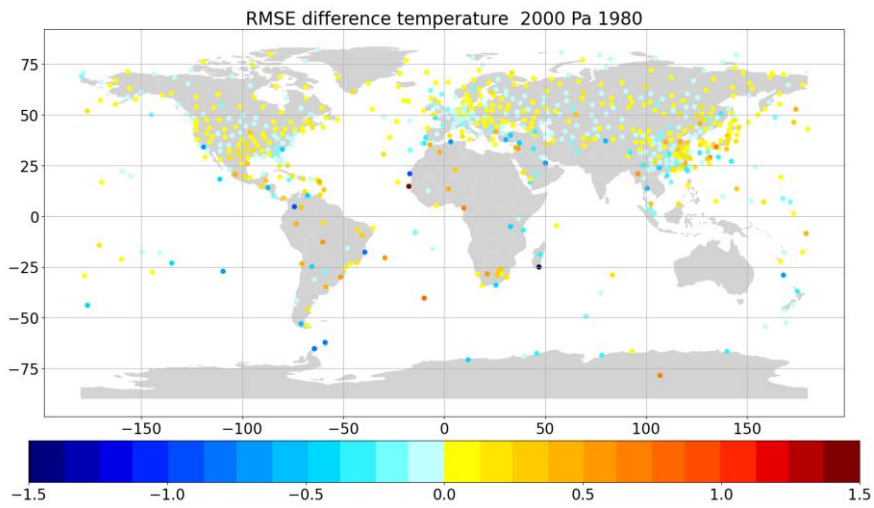
Figure 1344: Mean u wind [m/s] difference obs - ERA5 background at station position minus obs - ERA5 background at displaced position. All available values on 200 hPa of years 1991 - 2000.



592

593  
594  
595  
596

Figure 1445: Air temperature obs-bg RMSE difference for experiment "vertical" (orange) and for experiment "slanted" (red). The difference of differences (orange-red) yields the purple line, upper x axis, note scaling factor  $10^{-3}$ . Positive values indicate improvement due to more accurate balloon position. All available stations on mandatory pressure levels between 1980.06.01-1980.07.31.



597

598

599

600

Figure 1516: Air temperature obs-bg RMSE [K] difference of experiment “vertical” minus RMSE of experiment “slanted”. Positive values indicate improvement due to usage of more accurate balloon position. All available stations on 20 hPa between 1980.06.01-1980.07.31.

601 **Formula 1, 2: Calculation of the vertical gradient of temperature. See Table 1.**

602 
$$\Gamma(p) = \frac{\delta T}{\delta z} = \frac{\delta T}{\delta p} \frac{\delta p}{\delta z} = - \frac{\delta T}{\delta p^\kappa} \frac{\delta p^\kappa}{\delta p} \frac{\delta p}{\delta z}$$

603 (1)

604 
$$\Gamma(p) = - \frac{\delta T}{\delta p^\kappa} \frac{p^\kappa \kappa g}{T R_d} \quad \text{--- (2)}$$

605

606

607 **Formula 3: Calculation of layer height. See Table 1.**

608 
$$\Delta Z_{(i \rightarrow i+1)} = \frac{T_i}{\Gamma_i} \left( \frac{p_{i+1}}{p_i} \right)^{\frac{\Gamma_i R_d}{g} - 1}$$

609 (3)

610

611

612

**Table 1: Height profile calculation. Explanation of all used variables.**

Symbol	Description	Unit	Data source
$\Gamma$	temperature lapse rate	[K/m]	observed variable
$p$	pressure	[Pa]	observed variable
$T$	temperature	[K]	observed variable
$\Delta z$	layer height	[m]	calculated variable
$\square$	isentropic expansion factor	[1]	$\square = R/c_p$
$\square_\square$	specific heat capacity of air at constant pressure	[J/kg/K]	constant (1005.7)
$R_d$	gas constant for dry air	[J/kg/K]	constant (286.7)
$g$	standard gravity	[m/s <sup>2</sup> ]	constant (9.80665)

613

614

615 **Formula 4: Transport of the balloon with the wind. See Table 2.**

616 
$$\vec{S}_{(i+1)} = \vec{u}_{(i \rightarrow i+1)} * \frac{\Delta z_{(i \rightarrow i+1)}}{w_{balloon}}$$
  
617 (4)  
618  
619

620 **Table 2: Time interval calculation. Explanation of all used variables.**

Symbol	Description	Unit	Data source
$\vec{s}$	distance travelled	[m]	0 at i = 0, lon for u, lat for v
$\vec{u}$	wind	[m/s]	observed variable, u and v components of wind
$\Delta z$	layer height	[m]	calculated variable
w	rate of ascension	[m/s]	5, prescribed variable

621

622

623 **Table 3: Ascent speed percentiles for a sample of 10.000.000 observations with known altitude time series in 2020.**

Percentile	Value	Unit
1	2.05	[m/s]
5	2.82	[m/s]
25	4.01	[m/s]
75	5.85	[m/s]
95	7.74	[m/s]
99	10.09	[m/s]

624

625



626 Table 4: Statistics for the radiosonde observations actively used by both data assimilation experiments (vertical and slanted),  
627 separating between radiosondes launched from land stations and radiosondes launched from ships. P indicates the pressure (hPa),  
628 RSD indicates the robust standard deviation of background departures (i.e., before assimilation), SIGO indicates the estimated  
629 observation uncertainty (see text for details), and N indicates the data count. Results that differ between the two experiments are  
630 shown in bold and underlined. Observations that were used by only either one of the two experiments are excluded from these  
631 statistics.  
632

Pressure level range	P ≥ 500 hPa		500 hPa > P ≥ 100 hPa		100 hPa > P ≥ 1 hPa	
	Vertical	Slanted	Vertical	Slanted	Vertical	Slanted
<b>Radiosondes from land stations</b>						
<b>RSD</b>	1.2 K	1.2 K	1.3 K	1.3 K	<b><u>2.1 K</u></b>	<b><u>2.0 K</u></b>
<b>SIGO</b>	1.1 K	1.1 K	1.2 K	1.2 K	<b><u>2.1 K</u></b>	<b><u>2.0 K</u></b>
<b>N</b>	31,027,909	31,027,909	30,229,363	30,229,363	1,358,298	1,358,298
<b>Radiosondes from ships</b>						
<b>RSD</b>	1.2 K	1.2 K	1.2 K	1.2 K	<b><u>1.6 K</u></b>	<b><u>1.5 K</u></b>
<b>SIGO</b>	1.1 K	1.1 K	1.2 K	1.2 K	<b><u>1.8 K</u></b>	<b><u>1.6 K</u></b>
<b>N</b>	838,265	838,265	669,655	669,655	34,709	34,709

633  
634

635 **Code and data availability**

636 Radiosonde data used in the present work are available from <https://doi.org/10.7289/V5X63K0Q> (IGRA) and  
637 <https://doi.org/10.24381/cds.f101d0bf> (C3S CDS) and the [National Centers for Environmental Information \(NOAA](https://www.ncei.noaa.gov/data/ecmwf-global-upper-air-bufr/archive/https://weather.uwyo.edu/upperair/bufr/aob.shtml)  
638 [NCEI\) University of Wyoming Atmospheric Science](https://www.ncei.noaa.gov/data/ecmwf-global-upper-air-bufr/archive/https://weather.uwyo.edu/upperair/bufr/aob.shtml) Radiosonde Archive ([https://www.ncei.noaa.gov/data/ecmwf-global-](https://www.ncei.noaa.gov/data/ecmwf-global-upper-air-bufr/archive/https://weather.uwyo.edu/upperair/bufr/aob.shtml)  
639 [upper-air-bufr/archive/https://weather.uwyo.edu/upperair/bufr/aob.shtml](https://www.ncei.noaa.gov/data/ecmwf-global-upper-air-bufr/archive/https://weather.uwyo.edu/upperair/bufr/aob.shtml)). Climate reanalysis data (ERA5) are available from  
640 <https://doi.org/10.24381/cds.bd0915c6>. The code discussed in this paper is available from  
641 <https://doi.org/10.5281/zenodo.10663306><https://doi.org/10.5281/zenodo.8421009>.

642 **Author contribution**

643 Ulrich Voggenberger and Leopold Haimberger designed the method to estimate balloon positions. Ulrich Voggenberger  
644 developed the code and optimised the estimations and calculations with further input from Federico Ambrogio. Ulrich Leopold  
645 Haimberger and Ulrich Voggenberger ~~validated~~[verified](#) and evaluated the results based on ERA5 data. Paul Poli ran the data  
646 assimilation experiments and evaluated the results in section 6. Ulrich Voggenberger prepared the manuscript with  
647 contributions from all co-authors.

648 **Competing interests**

649 The contact author has declared that none of the authors has any competing interests.

650 **References**

- 651 [Aberson, S. D., Sellwood, K. J., & Leighton, P. A.: Calculating Dropwindsonde Location and Time from TEMP-DROP](#)  
652 [Messages for Accurate Assimilation and Analysis. In Journal of Atmospheric and Oceanic Technology \(Vol. 34, Issue](#)  
653 [8, pp. 1673–1678\). American Meteorological Society. <https://doi.org/10.1175/jtech-d-17-0023.1>, 2017.](#)
- 654 Alexander, P., and De La Torre, A.: Uncertainties in the measurement of the atmospheric velocity due to balloon-  
655 gondola pendulum-like motions. *Adv. Space Res.*, 47 (4):736-739, <https://doi.org/10.1016/j.asr.2010.09.020>, 2011.
- 656 [Choi, Y., J. Ha, and G. Lim, 2015: Investigation of the Effects of Considering Balloon Drift Information on Radiosonde](#)  
657 [Data Assimilation Using the Four-Dimensional Variational Method. \*Wea. Forecasting\*, 30, 809–826,](#)  
658 <https://doi.org/10.1175/WAF-D-14-00161.1> . 2015.
- 659 Crutcher, H. L.,: Distribution of radiosonde errors. NOAA Tech. Rep. Environmental Data and Information Service  
660 (EDIS), 32, [https://repository.library.noaa.gov/view/noaa/30830/noaa\\_30830\\_DS1.pdf](https://repository.library.noaa.gov/view/noaa/30830/noaa_30830_DS1.pdf), 1979.

661 Dabberdt, W. F., and Turtiainen, H.: Observations platforms: Radiosondes, in Encyclopedia of Atmospheric Sciences  
662 (Second Edition), eds. G. R. North, J. Pyle, F. Zhang, Academic Press, pp 273-284, ISBN 9780123822253.  
663 <https://www.sciencedirect.com/referencework/9780123822253/encyclopedia-of-atmospheric-sciences>, 2015.

664 Desroziers, G., Berre L., Chapnik B., and Poli, P.: Diagnosis of Observation, Background and Analysis-Error Statistics  
665 in Observation Space. Quarterly Journal of the Royal Meteorological Society 131, no. 613 (October 1, 2005): 3385–  
666 96. <https://doi.org/10.1256/qj.05.108.>, 2005.

667 Durre, I., Yin, X., Vose, R. S., Applequist, S., Arnfield, J., Korzeniewski, B., and Hundermark, B.: Integrated Global  
668 Radiosonde Archive (IGRA), Version 2. NOAA National Centers for Environmental Information.  
669 <https://doi.org/10.7289/V5X63K0Q>, 2016.

670 Dutton, J. A.: The ceaseless wind: An Introduction to the Theory of Atmospheric Motion. Dover Publications, New-  
671 York, 617 pp., ISBN:978-0486495033, <https://doi.org/10.1029/88EO01137>, 1986.

672 ECMWF: IFS Documentation CY48R1. <https://www.ecmwf.int/en/publications/ifs-documentation>, last access 25 Oct  
673 2023

674 Favà, V., Curto, J. J., and Gilibert, A.: Thermodynamic model for a pilot balloon, Atmos. Meas. Tech. ~~Discuss-~~  
675 [preprint], <https://doi.org/10.5194/amt-2021-206.>, 2021.

676 Gilpin, S., Rieckh, T., and Anthes, R.: Reducing representativeness and sampling errors in radio occultation–radiosonde  
677 comparisons, Atmos. Meas. Tech., 11, 2567–2582, <https://doi.org/10.5194/amt-11-2567-2018>, 2018.

678 Hersbach, H, Bell, B, Berrisford, P, et al.: The ERA5 global reanalysis. Q J R Meteor Soc. ~~2020-~~146: 1999–2049.  
679 <https://doi.org/10.1002/qj.3803>, ~~2020+~~999.

680 ICAO Standard Atmosphere - ISA <https://www.foehnwall.at/meteo/isa.html>, last access 25 Oct 2023

681 [Ingleby, B., P. Pauley, A. Kats, J. Ator, D. Keyser, A. Doerenbecher, E. Fucile, J. Hasegawa, E. Toyoda, T. Kleinert,](#)  
682 [W. Qu, J. St James, W. Tennant, and R. Weedon.: Progress toward High-Resolution, Real-Time Radiosonde Reports.](#)  
683 [Bull. Amer. Meteor. Soc., 97, 2149-2161, https://doi.org/10.1175/BAMS-D-15-00169.1. 2016.](#)

684 Ingleby, B., Isaksen, L., Kral, T., Haiden, Th., and Dahoui, M.: Improved use of atmospheric in situ data. ECMWF  
685 Newsletter 155. <https://doi.org/10.21957/cf724bi05s>, 2018.

686 Ingleby, B., Motl, M., Marlton, G., Edwards, D., Sommer, M., von Rohden, C., Vömel, H., and Jauhainen, H.: On the  
687 quality of RS41 radiosonde descent data, Atmos. Meas. Tech., 15, 165–183, <https://doi.org/10.5194/amt-15-165-2022>,  
688 ~~2022.~~

689 Kitchen, M.: Representativeness errors for radiosonde observations. Q. J. R. Meteorol. Soc., **115**: 673-700.  
690 <https://doi.org/10.1002/qj.49711548713>, 1989.

691 Laroche, S., and Sarrazin, R.: Impact of Radiosonde Balloon Drift on Numerical Weather Prediction and Verification.  
692 Weather and Forecasting, 28 (3), 772–782. <https://doi.org/10.1175/waf-d-12-00114.1>, 2013.

693 [McGrath, R., T. Semmler, C. Sweeney, and S. Wang.: Impact of balloon drift errors in radiosonde data on climate](#)  
694 [statistics. J. Climate, 19, 3430–3442, https://doi.org/10.1175/JCLI3804.1. 2006.](#)

695 Mears, C. A., and Wentz, F. J.: The effect of diurnal correction on the satellite-derived lower tropospheric temperature.  
696 Science, 309, 1548–1551. <https://doi.org/10.1126/science.1114772>, 2005.

697 Murillo, J., Mejia, J., Galvez, J., Orozco, R., and Douglas, M.: Quality control of pilot balloon network data for climate  
698 monitoring. Amer. Meteorol. Soc. 15th Conf. Appl. Clim., 13th Symp. Meteorol. Obs. Instr., **JPI.30** ,  
699 <https://api.semanticscholar.org/CorpusID:56365106>, 2005.

700 OpenStreetMap: OpenStreetMap® is open data, licensed under the Open Data Commons Open Database License  
701 (ODbL) by the OpenStreetMap Foundation (OSMF). You are free to copy, distribute, transmit and adapt our data, as  
702 long as you credit OpenStreetMap and its contributors. If you alter or build upon our data, you may distribute the result  
703 only under the same licence. The full legal code explains your rights and responsibilities. Our documentation is licensed  
704 under the Creative Commons Attribution-ShareAlike 2.0 license (CC BY-SA 2.0). Available from  
705 <https://planet.openstreetmap.org>, 2023.

706 Seidel, D. J., Sun, B., Petzey, M., and Reale, A.: Global radiosonde balloon drift statistics, J. Geophys. Res., 116,  
707 D07102, <https://doi.org/10.1029/2010JD014891>, 2011.

708 Singh, M., Kumar, B., Chattopadhyay, R., Amarjyothi, K., Sutar, A.K., Roy, S., Rao, S.A., and Nanjundiah, R.S.:  
709 Artificial intelligence and machine learning in earth system sciences with special reference to climate science and  
710 meteorology in South Asia. Current Sci., **122** (9), <https://doi.org/10.18520/cs/v122/i9/1019-1030>, 2022.

711 Steinacker, R., et al.: Unstationary aspects of Föhn in a large valley. Meteorology and Atmospheric Physics volume 92,  
712 pages 255–284 (2006). <https://doi.org/10.1007/s00703-005-0134-y>, 2005.

713 Stohl, A.: Computation, accuracy and applications of trajectories - A review and bibliography, Atmos. Env., **32** (6),  
714 [https://doi.org/10.1016/S1352-2310\(97\)00457-3](https://doi.org/10.1016/S1352-2310(97)00457-3), 1998

715 Tenenbaum, J., Williams, P.D., Turp, D., Buchanan, P., Coulson, R., Gill, P.G., et al.: Aircraft observations and  
716 reanalysis depictions of trends in the North Atlantic winter jet stream wind speeds and turbulence. Quarterly Journal of  
717 the Royal Meteorological Society, 148(747), 2927–2941. <https://doi.org/10.1002/qj.4342>, 2022.

718 Tschannett, S.: Objektive hochaufgelöste Querschnittsanalyse. Diplomarbeit, Univ. Wien,  
719 <https://www.univie.ac.at/img-wien/>, 2003.

720 WMO: Guide to Instruments and Methods of Observation Volume I: Measurement of Meteorological Variables ,  
721 Commission for Instruments and Methods of Observation (CI-MO) Guide, WMO Pub. 8. Available from  
722 <https://library.wmo.int/records/item/41650-guide-to-instruments-and-methods-of-observation>, 2021.

723 Zhang, J., Chen, H., Zhu, Y., Shi, H., Zheng, Y., Xia, X., Teng, Y., Wang, F., Han, X., Li, J., et al.: A Novel Method  
724 for Estimating the Vertical Velocity of Air with a Descending Radiosonde System. Remote Sens. **11**, 1538.  
725 <https://doi.org/10.3390/rs111131538>, 2019.

726